



CHORUS

This is the accepted manuscript made available via CHORUS. The article has been published as:

Torque Differential Magnetometry Using the qPlus Mode of a Quartz Tuning Fork

Lu Chen, Fan Yu, Ziji Xiang, Tomoya Asaba, Colin Tinsman, Benjamin Lawson, Paul M. Sass, Weida Wu, B. L. Kang, Xianhui Chen, and Lu Li

Phys. Rev. Applied **9**, 024005 — Published 7 February 2018

DOI: [10.1103/PhysRevApplied.9.024005](https://doi.org/10.1103/PhysRevApplied.9.024005)

Torque Differential Magnetometry Using the qPlus-Mode of a Quartz Tuning Fork

Lu Chen^{1,*}, Fan Yu¹, Ziji Xiang¹, Tomoya Asaba¹, Colin Tinsman¹, Benjamin Lawson¹, Paul. M. Sass², Weida Wu², B. L. Kang³, Xianhui Chen³, and Lu Li^{1†}

¹*Department of Physics, University of Michigan,
Ann Arbor, 450 Church Street, Ann Arbor, MI, 48108*

²*Department of Physics and Astronomy, Rutgers University,
136 Frelinghuysen Road, Piscataway, NJ 08854- 8019 and*

³*Hefei National Laboratory for Physical Science at Microscale and Department of Physics,
University of Science and Technology of China, Hefei 230026, China.*

(Dated: December 18, 2017)

Quartz tuning fork is the key component of high-resolution atomic force microscope. Because of its high quality factor, quartz tuning fork can also be used for high sensitivity magnetometry. Herein, we developed a highly sensitive torque differential magnetometry using the qPlus-mode of a quartz tuning forks. The tuning fork is driven by an AC voltage and its deflection is measured by the resultant AC current. We observed a sharp resonance of the quartz tuning fork at low temperature down to 1.6 K. We calibrated our torque differential magnetometry by measuring the angular dependence of the hysteresis loop in single crystalline Fe_{0.25}TaS₂. Furthermore, we demonstrated the high sensitivity of the torque differential magnetometry by measuring the quantum oscillations of bismuth single crystal. The extracted Fermi surface cross sections are consistent with those of bismuth crystals.

I. INTRODUCTION

Quartz resonators have been widely used as frequency standards in wrist watches due to its low internal dissipation and insensitivity to accelerations [1]. Among them, quartz tuning forks(QTF) are the most useful because of the surprisingly high quality factor (Q -factor) and low frequency variation at room temperature. Furthermore, the relatively high spring constant k_{eff} provides additional advantages like smaller oscillation amplitude [2] and larger linear operation range [3].

QTFs were introduced into scanning near-field acoustic microscopy as a new method for imaging the topography of nonconducting surfaces by Günther *et al* [4]. Later on, QTFs were used to fulfill tip-sample distance control in near-field optical microscopes [5]. Shear force detection was used in these microscopes and was explicitly investigated by Karrai and Tiemann [6]. Implementation of a tuning fork sensor suitable for high-resolution atomic force microscopy(AFM) imaging was achieved by involving phase lock loop(PLL) control [7]. By attaching a magnetic tip on a QTF, magnetic force microscopy can bring a spatial resolution of several tens of nanometers [8, 9]. Giessibl *et al.* also demonstrated a new configuration of QTF based AFM (called qPlus sensor) which maintains both high scanning speed and atomic resolution [10].

Apart from the application in scanning probe microscopy, QTFs have a potential for the high-sensitivity magnetometry due to high quality factor Q ($\sim 10^4$) and high sensitivity [11]. Cantilever-based torque magnetometry with resolution better than $10^4 \mu_B$ was widely used

to study small magnetization signal in magnetic thin layers [12] and individual nanotubes [13]. In these experiments, the read out of the magnetization signal usually involves mechanical oscillator drive and optical detection of cantilever deflection, often resulting in a cumbersome setup that is sensitive to the environment. It's necessary to develop an easy-to-set-up and highly sensitive magnetometry.

In the QTF-based torque magnetometry, magnetization coming from the sample generates a torque which changes the effective spring constant k_{eff} of the QTF. This change leads to a change in the resonance frequency. Thus it can be read out by its electrical response, such as current. Furthermore, cooling down to cryogenic temperature can effectively maximize the signal-to-noise ratio of the QTF[14][15]. This can, therefore, be a platform for a potentially easy-to-set-up sensitive magnetometry. However, QTF based torque magnetometry has not been widely studied and lacks thorough understanding. A major reason is that the quality factor is very sensitive to the mass of attached specimen and will drop dramatically when the two prongs are not well balanced, making it impractical for resonant detection. Previous QTF-based torque magnetometry was investigated with attaching an iron wire to one prong of a free tuning fork [11]. There are no prior studies on qPlus-mode magnetometry where one prong is mechanically fixed.

In this article, we demonstrate that a qPlus-like setup of QTF, dubbed torque differential magnetometry, can achieve several times larger Q than prior non qPlus-like setup even with a relatively massive sample [11]. The QTF device is integrated on the rotator probe of a Janis Variable Temperature Insert(VTI) system which provides a low temperature and vacuum environment. We tested two different measurement circuits and achieved high sensitivity measurements in both low and high mag-

* chelu@umich.edu

† luli@umich.edu

netic field. In order to calibrate the order of magnitude of magnetization measured with the quartz tuning fork, we measured the hysteresis loop of a well-studied ferromagnetic material $\text{Fe}_{0.25}\text{TaS}_2$ with different methods of magnetometry. Our analysis demonstrates that torque differential magnetometry can achieve a sensitivity which is comparable to that of the commercial Magnetic Property Measurement System (MPMS) as well as the cantilever-based torque magnetometer. Furthermore, we demonstrate the high sensitivity of our torque differential magnetometry by measuring the de Haas-van Alphen effect in the bismuth single crystal. Quantum oscillations are observed in a magnetic field up to 10 T and the extracted Fermi surfaces are consistent with previous results [16]. The observation of hysteresis loop, as well as the quantum oscillations, indicate that QTF-based magnetometry is a very promising characterization tool in studying the magnetic properties of many novel materials.

II. EXPERIMENTAL SETUP

Our experimental setup is shown in Figure 1 (a), one prong of the QTF is firmly glued on the side of an “L” shaped substrate with H74F epoxy from Epotek. Figure 1 (b) shows the side view of the experimental setup under the microscope. The “L” shaped substrate is machined from brass, which has high density and high thermal conductivity. Attaching a heavy mass to the tuning fork is crucial for obtaining a high quality factor. The sample is attached to the top of the free prong. The magnetic field is applied in the plane which formed by two crystalline axes (Inset of Figure 1 (b)). The QTFs (MS1V-T1K) are from Microcrystal with free standing resonance frequency $f_0 = 2^{15} \text{ Hz} = 32768 \text{ Hz}$. The original QTF is sealed in a metal case which holds a rough vacuum and can be gently removed with pliers. The spring constant of the quartz tuning fork can be calculated by the beam formula [17]

$$k = \frac{Et^3w}{4\Delta L^3}, \quad (1)$$

where E is Young’s modulus of quartz, t the thickness, w is the width, and ΔL is the effective length. After plugging in the numbers from reference [2, 17], $\Delta L = 2400 \mu\text{m}$, $t = 214 \mu\text{m}$, $w = 130 \mu\text{m}$ and $E = 79.1 \text{ GPa}$, the theoretical spring constant is approximately 1822 N/m. However, the calculation with the beam model is only a rough estimation for the spring constant and barely agree with the geometrical configuration of the qPlus sensors. The effective length $\Delta L = L - L_0$ is ambiguously defined since it highly depends on the mounting position L of the sample as well as the determination of the beam origin L_0 [18]. Furthermore, the assembling procedure, such as the non-symmetric alignment of the sample, will affect the spring constant of the QTF [19]. The rigid bonding between the sample and QTF, and between the QTF and substrate are crucial for obtaining a high Q

[20]. The whole device is tightly fixed on a 16 pin socket which seats on the rotator probe of a Janis VTI system and stays in vacuum during the whole measurement.

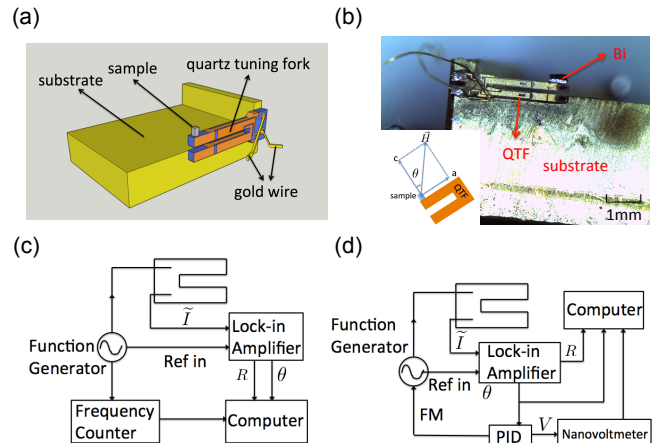


Figure 1. (a) Experimental setup. One prong of the QTF is firmly glued on the side of an “L” shaped substrate. The sample is attached on top of the free prong. (b) Side view of the experimental setup under the microscope. Inset shows the sketch of the measurement setup, where the magnetic field is applied in the ac plane of the sample. The sample stage is rotatable up to 90 degrees. θ is the angle between the c axis and H . Schematic of the experimental circuit: (c) direct mode and (d) PLL mode.

In our experiments, we performed frequency dependent current measurements with the direct mode circuit shown in Figure 1 (c). A KEYSIGHT 33520B function generator is used to provide a 10mV AC voltage across the QTF. The signal frequency is read by a KEYSIGHT 53230A frequency counter. At the same time, the responding current $\tilde{I}(\omega)$ due to piezoelectric effect is measured with a Stanford Research 830 lock-in amplifier whose reference signal comes from the function generator.

The field dependent current measurement is achieved with both the direct mode circuit and phase lock loop(PLL) mode circuit (Figure 1 (d)). In direct mode, the frequency of the function generator is always fixed at the resonance frequency of the QTF at zero field. When the magnetic field is changing, the magnetization in the sample generates a torque on the free prong of the QTF, which modifies the resonance frequency of the QTF. The lock-in amplifier measures the amplitude and phase of the current through the QTF. All data acquisition is fulfilled by Labview programming.

The phase shift of the current depends on how much the resonance frequency deviates from the excitation frequency. Compared with the direct mode, the PLL mode [7] can directly measure the frequency change of the QTF when applying a field. The shift of the QTF is quite steep at the resonance frequency [11] because of high Q factor.

This slope can be used to convert the phase signal to the frequency change. In the PLL mode measurement, the drive frequency of QTF is modulated by a feedback loop to maintain constant phase. The phase lock loop is achieved by sending the phase of the current to the input of a Stanford Research SIM960 analog PID controller, while the output of the PID is used to modulate the frequency of the function generator and is recorded by a Keithley 2182A nanovoltmeter.

III. TORQUE DIFFERENTIAL MAGNETOMETRY

In our experiment, the magnetization from the sample is represented by the frequency change of the QTF. Here we give a brief mechanical model which is similar to the mechanism of the frequency-modulated cantilever magnetometry [21]. In the qPlus configuration, only one prong of the QTF can oscillate freely while the other prong is tightly fixed on the substrate. The free prong is equivalent to a quartz cantilever which performs harmonic oscillation when applying AC voltage. In the PLL mode, the QTF is driven at its resonance frequency ω_0 during the measurement. The displacement of the free prong is given by $x(t) = x_0 \cos(\omega_0 t)$. In the presence of an external magnetic field H , the magnetization M from the sample applies a torque $\tau = M \times H$ on the QTF. The motion of the QTF can be expressed by

$$m_{\text{eff}} \frac{d^2 x}{dt^2} + \gamma \frac{dx}{dt} + k_{\text{eff}} x = F_{\text{drive}} + F_{\tau}, \quad (2)$$

in which m_{eff} is the effective mass of the free prong, γ is the damping factor, k_{eff} is the effective spring constant, F_{drive} is the driving force and F_{τ} is the force coming from the magnetic torque. F_{τ} can be further expressed as $F_{\tau} = \tau/L_{\text{eff}}$, where L_{eff} is the effective length of the QTF. Here we define the angle between H and c axis to be the tilt angle θ . While the free prong keeps on oscillating, the motion adds a small oscillation change to the θ which makes $\theta'(t) = \theta + \Delta\theta(t)$. $\Delta\theta(t)$ also varies with the same frequency ω_0 of the driving force and can be written as $\Delta\theta(t) = \Delta\theta_0 \cos(\omega_0 t)$, in which $\Delta\theta_0$ relates to the oscillation amplitude of the free prong $\Delta\theta_0 = x_0/L_{\text{eff}}$. In other words, the deflection of QTF (x) is $\Delta\theta(t) = x(t)/L_{\text{eff}}$. The force change can be expanded as

$$F_{\tau}(\theta + \Delta\theta(t)) - F_{\tau}(\theta) \approx \frac{\partial F_{\tau}}{\partial \theta} \Delta\theta(t) = \frac{1}{L_{\text{eff}}} \frac{\partial F_{\tau}}{\partial \theta} x(t) \quad (3)$$

Therefore, the magnetic torque results in a change of effective spring constant

$$\Delta k_{\text{eff}} = k'_{\text{eff}} - k_{\text{eff}} = \frac{1}{L_{\text{eff}}} \frac{\partial F_{\tau}}{\partial \theta} = \frac{1}{L_{\text{eff}}^2} \frac{\partial \tau}{\partial \theta}, \quad (4)$$

So the shift of the resonance frequency becomes

$$\Delta\omega_0 \approx \omega_0 \frac{\Delta k_{\text{eff}}}{2k_{\text{eff}}} = \frac{\omega_0}{2L_{\text{eff}}^2 k_{\text{eff}}} \frac{\partial \tau}{\partial \theta}, \quad (5)$$

Therefore, in PLL mode the frequency shift is proportional to the derivative of the magnetic torque with respect to the tilt angle θ , which means the quartz tuning fork is actually a torque differential magnetometer [3].

When the magnetic field is applied in the ac plane of the crystal (Inset of Figure 1 (b)), the magnetic torque can be expressed with the components along crystalline c and a axis by

$$\tau = M_a H_c - M_c H_a. \quad (6)$$

For a paramagnetic or diamagnetic material [22],

$$\begin{aligned} \tau &= \mu_0 \chi_a H_a H_c - \mu_0 \chi_c H_c H_a \\ &= \mu_0 \Delta\chi H^2 \sin\theta \cos\theta, \end{aligned} \quad (7)$$

where μ_0 is the vacuum permeability and $\Delta\chi = \chi_a - \chi_c$ is the magnetic susceptibility anisotropy. With the same derivation, the frequency shift for a paramagnet material is

$$\Delta\omega_0 \approx \omega_0 \frac{\mu_0 \Delta\chi H^2 \cos 2\theta}{2L_{\text{eff}}^2 k_{\text{eff}}} = \omega_0 \frac{M_{\text{eff}} H \cos 2\theta}{2L_{\text{eff}}^2 k_{\text{eff}}}, \quad (8)$$

in which $M_{\text{eff}} = \mu_0 \Delta\chi H$ is the effective magnetization.

If the sample is not paramagnetic along all crystal axes, the θ dependence of the frequency shift is a little bit different. Take $\text{Fe}_{0.25}\text{TaS}_2$ as an example, it is a paramagnet along a axis but a ferromagnet along c axis [23]. When the magnetization along c axis is saturated, the magnetic torque can be written as

$$\tau = \frac{1}{2} \mu_0 \chi_a H^2 \sin 2\theta - M_s H \sin\theta, \quad (9)$$

in which M_s is the saturation magnetization along c axis. In $\text{Fe}_{0.25}\text{TaS}_2$, the magnetization in ab plane is very low compared with the saturation magnetization along c axis [23]. As a result, the frequency shift is following

$$\Delta\omega_0 = \omega_0 \frac{\mu_0 \chi_a H^2 \cos 2\theta}{2L_{\text{eff}}^2 k_{\text{eff}}} - \omega_0 \frac{M_s H \cos \theta}{2L_{\text{eff}}^2 k_{\text{eff}}}. \quad (10)$$

Further, given the magnetic torque is dominated by the second term in Eq. (9), the dominating term in Eq. (10) would be the second term, which means the frequency shift is proportional to H . Later we are going to demonstrate the angular dependence of the frequency shift at H_c in $\text{Fe}_{0.25}\text{TaS}_2$ single crystal.

IV. RESULTS

A. Hysteresis Loop in $\text{Fe}_{0.25}\text{TaS}_2$

In order to calibrate the order of magnitude of the magnetic moment measured by the quartz tuning fork as well as verify the theoretical model of torque differential magnetometry, we measured the hysteresis loop of a well-studied ferromagnetic material $\text{Fe}_{0.25}\text{TaS}_2$ with different methods of magnetometry. The $\text{Fe}_{0.25}\text{TaS}_2$ sample used

here were grown by chemical vapor deposition method [24]. Both the magnetization and resistivity are extremely anisotropic, with the magnetic moments aligned parallel to the c crystallographic direction [23–25].

Anisotropic magnetization was taken by a Quantum Design Physical Property Measurement System (PPMS) using the Vibrating Sample Magnetometer (VSM) option at 1.9 K. The sample measured in PPMS (sample A) has a dimension of $0.9 \text{ mm} \times 0.75 \text{ mm} \times 0.05 \text{ mm}$. As shown in figure 2 (a), a sharp hysteresis loop was observed when $H \parallel c$. The $H \parallel c$ magnetization saturates at 5.2 T ($M_s \sim 10^{-3} \text{ emu}$) and is about 1 order of magnitude larger than the $H \parallel ab$ magnetization ($M_{ab} \sim 10^{-4} \text{ emu}$).

The angular dependent magnetic torque of sample B was measured by the cantilever-based torque magnetometer. The experimental setup is similar to the one in reference [22], a $0.3 \text{ mm} \times 0.16 \text{ mm} \times 0.05 \text{ mm}$ single crystal was put on the tip of a beryllium copper cantilever with a magnetic field applied in the ac plane. The magnetic torque τ coming from the sample is measured by tracking the capacitance change between the cantilever and a gold film underneath [26]. Figure 2 (b) shows the torque vs. H at $\theta = -34.8^\circ$, in which θ is the angle between H and c axis. The bow-tie feature corresponds to the sharp jump in the magnetization at the coercive field H_c . As demonstrated in the previous session, the magnetic torque in this material is dominated by the second term in Eq. (9). So the torque signal should be proportional to $\sin\theta$. The loop height was defined as the torque change at the coercive field $\tau_c = \tau_c^{\text{up}}(H_c) - \tau_c^{\text{down}}(H_c)$. The angular dependent torque measurement was done from -45° to 45° . The angular dependent data shows that the loop closes exactly at $\theta = 0^\circ$ and the loop size gradually increases as θ deviates from 0° (Figure 2 (e)). Theoretically, the torque signal should get a maximum at $\theta = \pm 45^\circ$. Unfortunately, we were not able to get the angular dependence above 45° due to the limitation of our rotator. The angular dependent $\Delta\tau_c/2H_c$ data can be well fitted with Eq. (9) (red dashed line in Figure 2 (e)), which indicates the magnetization from the c axis is about 45 times larger than the contribution from the ab plane. In comparison, we also fit the angular dependent data with a sinusoidal function (blue dashed line). It turns out that with a large magnetic anisotropy, $\text{Fe}_{0.25}\text{TaS}_2$ can be approximated with a 3D Ising model.

Sample B was then attached on the free prong of a qPlus-mode quartz tuning fork with the magnetic field applied in the ac plane. The field dependent frequency shift was measured by the PLL mode and the frequency shift vs H at $\theta = -38^\circ$ was shown in figure 2 (c). A similar hysteresis loop with a bow-tie feature was observed. Here the loop height is defined as the frequency shift jump at the coercive field $\Delta f_c = f_c^{\text{up}}(H_c) - f_c^{\text{down}}(H_c)$, the loop width is defined as $2H_c$. The angular dependent hysteresis loops show that the loop height gets a maximum at $\theta = 0^\circ$ and continuously increases as θ deviates from 0° . Figure 2 (d) shows the angular dependent $\Delta f_c/2H_c$, which can be well fitted with Eq. (10)

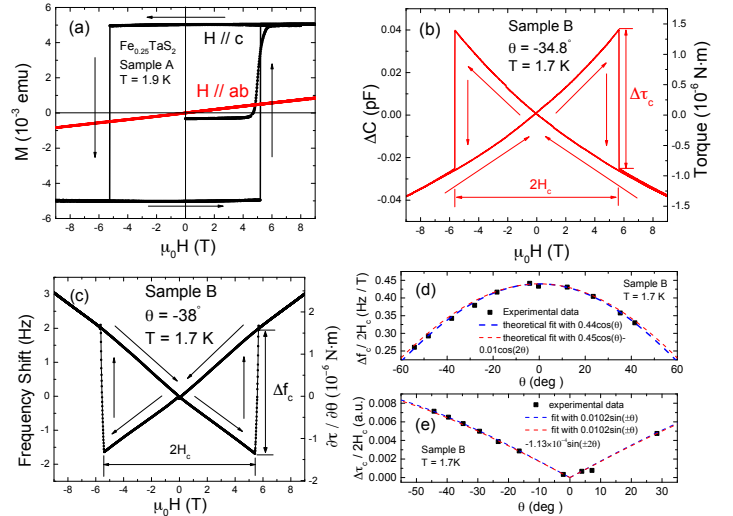


Figure 2. Hysteresis loop in $\text{Fe}_{0.25}\text{TaS}_2$. (a) $M(H)$ curves for $H \parallel c$ (black) and $H \parallel ab$ (red) measured by VSM in sample A at 1.9 K. (b) Torque vs. H measured by torque magnetometer in sample B at 1.7 K. (c) Frequency shift vs. H measured by quartz tuning fork in sample B at 1.7 K. θ is the angle between H and c axis. The differential of torque is derived with Eq. (5). Arrows here denote the direction of magnetic field change. (d) $\Delta f_c/2H_c$ vs θ for the quartz tuning fork. (e) $\Delta\tau_c/2H_c$ vs θ for the cantilever. Blue dashed lines are the theoretical fitting with the magnetization only along the c axis. Red dashed lines are theoretical fitting with magnetization coming from both c axis and ab plane.

(red dashed line). The magnetic anisotropy derived from the fitting is consistent with the result of the cantilever data (Figure 2 (e)). If we treat the $\text{Fe}_{0.25}\text{TaS}_2$ sample as a 3D Ising system, the angular dependence of $\Delta f_c/2H_c$ can be well fitted with the second term of Eq. (10) (blue dashed line). This angular dependent behavior verifies that tuning fork is actually measuring the differentiation of magnetic torque instead of the torque itself. The coefficient in front of the $\cos\theta$ in the fitting function equals to $\frac{f_0 M_s}{2L_{\text{eff}}^2 k_{\text{eff}}}$. The resonance frequency f_0 of the QTF with $\text{Fe}_{0.25}\text{TaS}_2$ sample attached is 30432 Hz, the effective length of QTF is $L_{\text{eff}} = 2.4 \text{ mm}$, the saturation magnetization is $M_s = 3.55 \times 10^{-7} \text{ emu}$. Then the spring constant can be calculated to be $k = 2131 \text{ N/m}$ after plugging in all these numbers, which is consistent with the calculated spring constant in previous session and the reported values ($10^3 \sim 10^4 \text{ N/m}$) in previous studies [10, 17, 27, 28].

B. Quantum Oscillations in Bismuth

We also did the field dependent measurement for single crystal bismuth (Bi) with the qPlus-mode QTF. The orientation of the bismuth crystal is confirmed by X-ray diffraction. A $0.6 \text{ mm} \times 0.2 \text{ mm} \times 0.13 \text{ mm}$ (~ 156

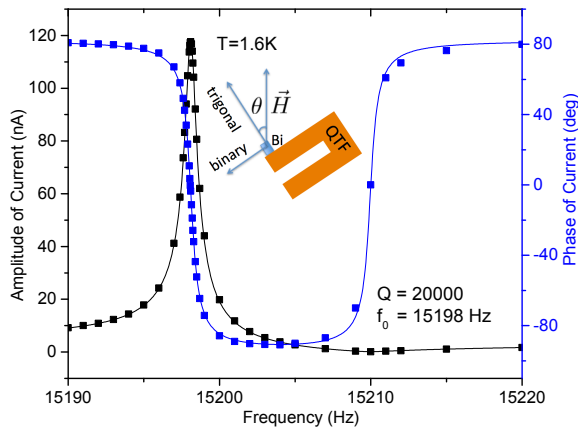


Figure 3. Resonance curve of the QTF with Bi sample attached at 1.6 K and in the vacuum. $Q = 20000$, $f_0 = 15198$ Hz. Inset is the configuration of the measurement. The magnetic field is applied in the trigonal-binary plane of the Bi crystal.

μg) bismuth (Bi) crystal is attached on the top of the free prong. The zero field resonance curve was measured with the direct mode at 1.6 K, as shown in Figure 3. The amplitude of the current shows a sharp peak at resonance frequency f_0 while the slope of the phase curve is quite steep. Fitting the magnitude and the phase of the current with Eq. (1) and (2) in reference [27] gives a quality factor around 20000 and $f_0 = 15198$ Hz. The phase of the current has a linear relationship with the frequency within ± 0.3 Hz around f_0 , so we can use the phase deviation to infer the shift of the resonance frequency Δf if $f_0 + \Delta f$ was in this linear range. However, strong magnetic torque in a high field could result in large frequency shift beyond the linear range. In this situation, the PLL mode has to be involved to track the variation of f_0 in a broad range.

To verify that the direct mode can produce the same result as the PLL mode in this linear range, field dependent measurements up to 10 T are performed with both modes. The crystal orientation is shown in the inset of Figure 3, the magnetic field is rotating in the trigonal-binary plane of the Bi crystal, θ denotes the angle between the field and the trigonal axis. Figure 4 (a) and (b) show that the frequency shift in the PLL mode and the phase of the current in the direct mode shows the same pattern (later we will compare the periodicity to $1/\mu_0 H$). Figure 4 (c) is the effective magnetization M_{eff} calculated from the frequency shift with Eq. (8). Comparing Figure 4 (a) with Figure 4 (b), the direct mode is better at revealing high pitch oscillations with respect to $\mu_0 H$ at low field. The reason is when the magnetic field changes, the magnetization of the sample changes the resonance frequency of the QTF and produces a phase shift on the current. With a sweeping rate of 0.23 T per minute, to obtain a stable PLL, the integration gain can not be too large, which means the time constant of the PLL can not

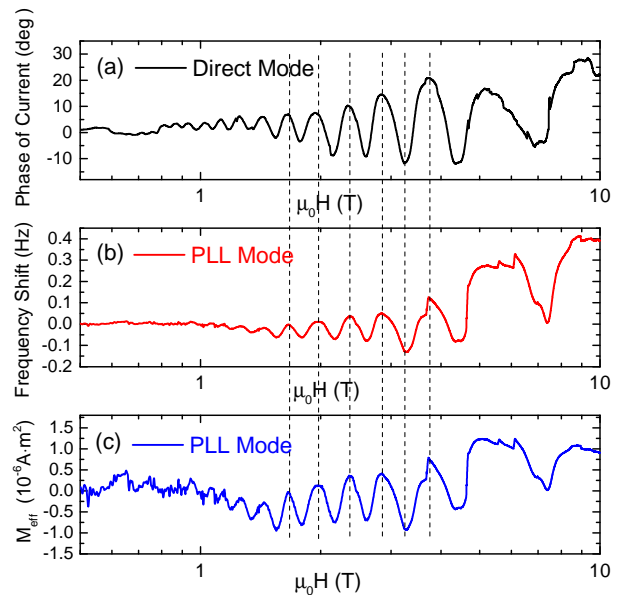


Figure 4. Quantum oscillations observed in the Bi crystal with two different measurement modes: (a) The phase of the current vs. H in direct mode. (b) Frequency shift vs. H in PLL mode. (c) Converted effective magnetization M_{eff} vs. H with Eq. (8) in PLL mode. Here we used $k = 2131$ N/m from the fitting result of angular dependent $\text{Fe}_{0.25}\text{TaS}_2$ data for calculating M_{eff} . M_{eff} signal is quite noisy at low field. This is because M_{eff} is calculated through dividing the frequency shift by H , which is comparably a larger number at low field. All curves are taken at $\theta = -43^\circ$, 1.6 K. Dashed lines are given as guides to the eye.

be too small. The PID takes quite a long time to gradually reach a stable output which tunes the frequency of the function generator to the new resonance frequency. However, before the PID generates a stable output, the variation of magnetization forces it to achieve a new resonance frequency. So the direct mode has advantages in low field measurements since the phase of the current always responds more rapidly than the PID output.

In our experiment, we performed angular dependent measurements up to 10 T at 1.6 K. Figure 5 shows the raw data taken with the direct mode at 6 selected angles. When H is increasing, the Landau level energies are also increasing. Every time the Fermi surface passes through a Landau level, the derivative of free energy F over H has an extreme slope. Hence the Landau level crossings can be observed as a series of anomalies in the phase of the current versus H . If H was at an angle α to the normal direction of a Fermi surface, the extreme slope happens at fields B_n given by [29]

$$\frac{1}{B_n} = \frac{2\pi e}{\hbar} (n + \gamma) \frac{1}{S(\alpha)}, \quad (11)$$

where \hbar denotes the reduced Plank constant, e is the electrical charge, n is a positive integer, γ is the Onsager phase, and $S(\alpha)$ is the Fermi surface cross section at the magnetic field tilt angle α . We use (n, \pm) to denote the

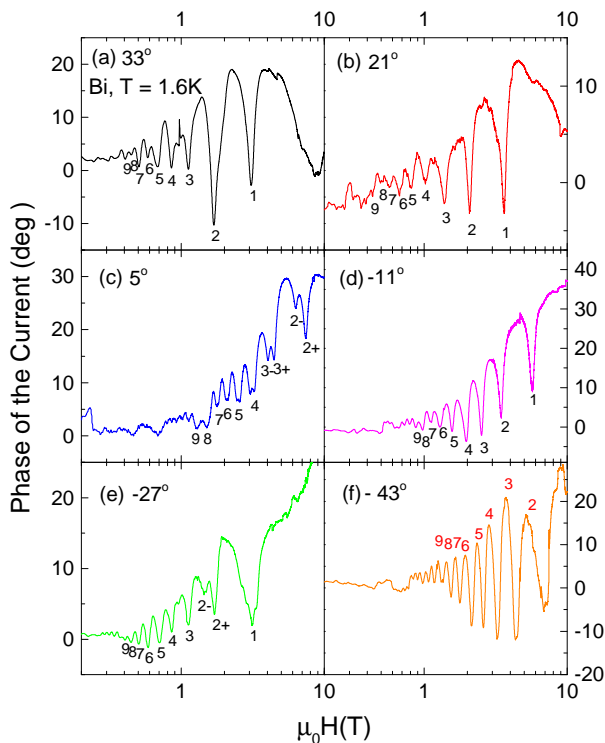


Figure 5. The phase of the current vs. H of the Bi crystal at six selected angles taken at 1.6 K (H is in log scale) with direct mode. Crossings of the Landau sublevels (n, s) appear as extremes B_n in the phase of the current. ($n, +$) and ($n, -$) denote the splitting of degenerate Landau levels due to the Zeeman effect.

sub-Landau levels due to Kramers degeneracy. For the electron pocket, the index field B_n is distinguished by a minimum in the phase of the current, as shown in Figure 5 (a) - (e). For the hole pocket, B_n is revealed by peaks in the phase of the current, as shown in Figure 5 (f).

Landau level indices n vs. $1/B_n$ measured at three selected angles are plotted in Figure 6 (a). For the hole pocket, eg. $\theta = -43^\circ$, the data points fall on a straight line which has an intercept of 0 as H approaches infinity. Whereas for the electron pocket, eg. $\theta = -11^\circ, 33^\circ$, the infinite field limit of the index plot intercept is around -0.2. This linear relationship confirms that the above indexing is consistent, the slope corresponds to the dominant quantum oscillation frequency at each angle, from which we can extract the Fermi surface cross-section projected on the plane perpendicular to H .

At each angle, quantum oscillations could come from both electron and hole pockets. Multi-frequencies of the quantum oscillations are revealed by the fast Fourier transform (FFT) of the field dependent phase data. A polynomial background has been subtracted before the FFT process. Figure 6 (b) shows the angular dependence of the quantum oscillation frequencies which can be fit with a 3D ellipsoidal Fermi surface model [29]. Red dashed lines denote quantum oscillation periods coming

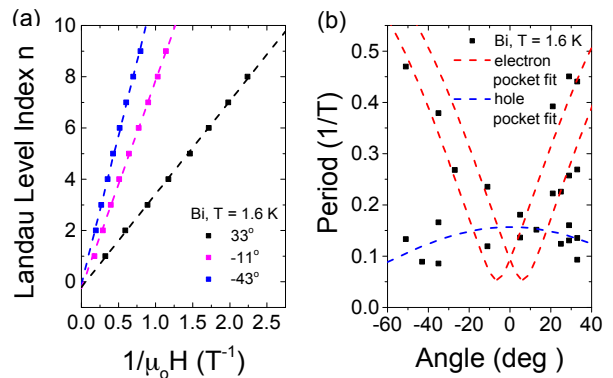


Figure 6. (a) Plot of the Landau level index n vs. $1/B_n$ at three selected angles. The Landau levels all fall on straight lines. The slopes give Fermi surface cross-section areas S_e at corresponding angles. (b) Oscillation periods of the observed Fermi surfaces is shown as a function of the angle between H and trigonal axis. Dashed lines are theoretical fittings from -60° to 40° with a 3D ellipsoidal Fermi surface model. Red dashed lines represent two electron pockets while a blue dashed line denotes the hole pocket.

from two electron pockets which are symmetric with respect to the bisectrix axis. The blue dashed line represents the periods originating from the hole pocket that extends along the trigonal axis. Our results are consistent with previous de Haas-van Alphen measurements in Bi [16]. In the cantilever-based torque magnetometry measurement done by Li. *et al.* [30], the Bi sample has a mass of 0.12 g (770 times larger than our sample) and the quantum oscillation starts to show up at $B \sim 0.5$ T. With a much smaller sample, a quantum oscillation is revealed at a comparable magnetic field in our experiment, which indicates QTFs have advantages in small signal detection.

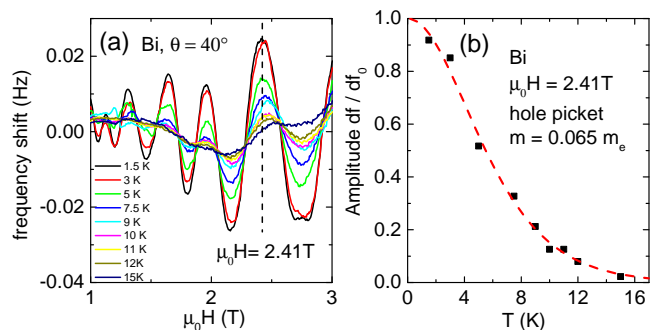


Figure 7. Temperature dependence of oscillating frequency shift for Bi. (a) Frequency shift after subtracting a polynomial background is plotted at T between 1.5 K and 15 K. θ is the angle between H and the trigonal axis. (b) Temperature dependence of the oscillating frequency shift at $\mu_0 H = 2.41$ T, normalized by the 0 K limit. Fitting the oscillating amplitude to the LK formula (red dashed line) yields the effective mass $m = 0.065 m_e$ for the hole pocket.

The electronic properties of Fermi surfaces can be revealed by tracking the temperature dependence and the magnetic field dependence of the quantum oscillation amplitude, which is well defined by the Lifshitz-Kosevich (LK) formula [29]. The oscillation amplitude is determined by the product of thermal damping factor R_T and Dingle damping factor R_D , as follows,

$$R_T = \alpha T m^* / B \sinh(\alpha T m^* / B), \quad (12)$$

$$R_D = \exp(-\alpha T_D m^* / B), \quad (13)$$

where the effective mass $m = m^* m_e$ and the Dingle temperature $T_D = \hbar / 2\pi k_B \tau_S$. m_e is the bare electron mass, τ_S is the scattering rate, k_B is the Boltzmann Constant, and $\alpha = 2\pi^2 k_B m_e / e\hbar \sim 14.69$ T/K. Figure 7 (a) shows the temperature dependent frequency shift after subtracting a polynomial background between 1.5 K and 15 K. Fitting the temperature dependence of the normalized frequency shift at $\mu_0 H = 2.41$ T yields $m = 0.065 m_e$ for the hole pocket, which is within 20% error of the reported value in ref. [31].

V. DISCUSSION

The frequency sensitivity of the direct mode can be estimated in the following way. From the resonance curve of QTF with Bi sample attached (Figure 3), the slope of the phase vs. frequency is 132 deg./Hz. The main uncertainty of the direct mode measurement depends on the uncertainty of the phase measured by the lock-in amplifier. In our setup, the error from the phase measured by the lock-in is ± 0.5 deg, which means the frequency sensitivity is about ± 3.8 mHz. This is about 7 ~ 8 times higher than the frequency sensitivity achieved by the free tuning fork magnetometer [11].

As for the PLL mode, the major limitation for the sensitivity comes from the output of PID. Take the hysteresis loop measurement as an example, the uncertainty for the PID output is about 3×10^{-3} V, which corresponds to 1.8×10^{-3} Hz. The sensitivity of the saturation magnetization is estimated to be $\delta M_s \sim 2.8 \times 10^{-10}$ A·m² $\sim 2.8 \times 10^{-7}$ emu at 5 T, which is comparable to the claimed best sensitivity of the latest MPMS (sensitivity $\sim 5 \times 10^{-8}$ emu) by Quantum Design. With the magnitude of our magnetic moment signal about 10^{-4} emu, the signal to noise ratio for our setup is 10^3 . The sensitivity of QTF-based differential torque magnetometer is comparable to the sensitivity of cantilever-based torque magnetometer used for the hysteresis loop measurements. In our torque magnetometer experiment, the uncertainty of the beryllium-copper cantilever's capacitance is about 10^{-5} pF, which corresponds to a magnetic moment of 1×10^{-7} emu at 5 T. In the cantilever-based torque magnetometry, a thinner cantilever beam can achieve a higher sensitivity (10^{-10} emu). This is because a thinner beam has a lower spring constant, which makes the relative

capacitance change ($\Delta C/C_0$) larger and has higher sensitivity. But it would not sustain the rather large torque signal from the ferromagnet (10^{-4} emu). Finally, we note that the majority of the frequency noise comes from the commercial analog PID feedback controller used in our electronics. In the future study, the performance and sensitivity of torque differential magnetometry can be improved by using a dedicate PLL with tunable bandwidth. The magnitude of M_s for Fe_{0.25}TaS₂ sample B is about 10^{-4} emu, so the signal to noise ratio for our setup is 10^3 .

The frequency sensitivity in the PLL mode is higher compared to the sensitivity in the direct mode, which is counterintuitive at the first glance. This is because the qPlus-mode QTF with Fe_{0.25}TaS₂ sample attached has a 2.25 times larger Q compared to the QTF with Bi sample attached. As an approximate estimation, the slope of the phase curve for Fe_{0.25}TaS₂ sample will be around ± 297 deg./Hz. This results in a frequency sensitivity about ± 1.68 mHz, which is smaller than the frequency sensitivity in the PLL mode (1.8 mHz). This comparison indicates that a higher Q can help a lot in increasing the sensitivity of the direct mode.

Apart from the DC magnetic field, QTFs could potentially be used in a pulsed field up to 65 T as well. As an insulator, quartz does not have a problem with eddy currents present in metal cantilevers. Furthermore, the resonance frequency of the QTF is much higher than that of the traditional cantilever ($\lesssim 100$ Hz), which reduces the coupling between the QTF signal and low frequency mechanical vibration coming from the environment. The response time of magnetometry needs to be much smaller than the ring up time of the pulsed field (about 8 ms). Therefore, a QTF with higher resonance frequency is desirable in the pulsed field measurement.

In conclusion, we developed a qPlus-like setup for torque differential magnetometry with the QTF. With the sample attached, the QTF maintains an excellent Q factor of $\sim 10^4$ at 1.6 K. Two different circuits for low and high field measurements maintain high sensitivity in both conditions. The hysteresis loop measurement in the ferromagnetic Fe_{0.25}TaS₂ single crystal proves that QTF can achieve a sensitivity of magnetic moment measurement at around 10^{-7} emu, which is comparable to other state-of-the-art magnetometers. The field dependent measurement on the well-studied metal Bi gives solid evidence for the observation of quantum oscillations. Our measurements on ferromagnet and quantum oscillations demonstrated that our qPlus QTF magnetometry is a reliable method for conducting torque differential magnetometry measurements, especially at cryogenic temperatures and intense magnetic fields. Since the magnetic torque is the derivative of the free energy with respect to the tilt angle, the qPlus QTF magnetometry measures the second derivative of the free energy with respect to the tilt angle, thus providing a powerful probe to resolve the electronic and magnetic anisotropy of novel solid state materials.

Acknowledgements This work is mainly supported

by the US Department of Energy under Award No. DE-SC0008110 (magnetization measurement). Supporting measurements were made possible with the support by the Office of Naval Research through the YIP award No. N00014-15-1-2382 (thermal and electrical characterization), and the National Science Foundation MRI award under No. DMR-1428226 (supports the equipment). We

thank Ctirad Uher for providing Bi single crystals. T.A. thanks the Nakajima Foundation for support. W.W. and P.M.S. were supported by the US DOE award No. DE-SC0008147. B. L. Kang and X. Chen were supported by the National Key R&D Program of the MOST of China (Grant No. 2016YFA0300201) and the Nature Science Foundation of China (Grant No. 11474287).

-
- [1] Piezoelectric Quartz Tuning Forks for Scanning Probe Microscopy, 2005, Nanonis GmbH, Switzerland.
- [2] F.J. Giessibl, S. Hembacher, M. Herz, C. Schiller, J. Mannhart, Stability considerations and implementation of cantilevers allowing dynamic force microscopy with optimal resolution: the qPlus sensor, *Nanotechnology* **15**, S79 (2004)
- [3] A. Kamra, M. Schreier, H. Huebl, and S. T. B. Goennenwein, Theoretical model for torque differential magnetometry of single-domain magnets, *Phys. Rev. B* **89**, 184406 (2014)
- [4] P. Günther, U. Ch. Fischer, and K. Dransfeld, Scanning near-field acoustic microscopy, *Appl. Phys. B* **48**, 89 (1989)
- [5] K. Karrai and Robert Grober, Piezoelectric tip-sample distance control for near field optical microscopes, *Appl. Phys. Lett.* **66**, 1842 (1995)
- [6] K. Karrai and I. Tiemann, Interfacial shear force microscopy, *Phys. Rev. B* **62**, 13174 (2000)
- [7] H. Edwards, L. Taylor, W. Duncan, and A. J. Melmed, Fast, high-resolution atomic force microscopy using a quartz tuning fork as actuator and sensor, *J. Appl. Phys.* **82**, 980 (1997)
- [8] Y. Martin and H.K. Wickramasinghe, Magnetic imaging by force microscopy with 1000 Å resolution, *Appl. Phys. Lett.* **50**, 1455 (1987).
- [9] M. R. Koblischka, U. Hartmann, and T. Sulzbach, Resolving magnetic nanostructures in the 10-nm range using MFM at ambient conditions, *Mater. Sci. Eng. C* **23**, 747 (2003).
- [10] F. J. Giessibl, High-speed force sensor for force microscopy and profilometry utilizing a quartz tuning fork, *Appl. Phys. Lett.* **73**, 3956 (1998)
- [11] A. Kamra, S.V. Hoesslin, N. Roschewsky, J. Lotze, M. Schreier, R. Gross, S. T. B. Goennenwein, and H. Huebl, An all-electrical torque differential magnetometer operating under ambient conditions, *Eur. Phys. J. B* **88**, 224 (2015)
- [12] B.C. Stipe, H.J. Mamin, T.D. Stowe, T.W. Kenny, D. Rugar, Magnetic Dissipation and Fluctuations in Individual Nanomagnets Measured by Ultrasensitive Cantilever Magnetometry, *Phys. Rev. Lett.* **86**, 2874 (2001)
- [13] D. P. Weber, D. Ruffer, A. Buchter, F. Xue, E. Russo-Averchi, R. Huber, P. Berberich, J. Arbiol, A. Fontcuberta i Morral, D. Grundler, and M. Poggio, Cantilever Magnetometry of Individual Ni Nanotubes, *Nano Lett.* **12**, 6139 (2012)
- [14] Franz J. Giessibl, Florian Pielmeier, Toyooki Eguchi, Toshi An, Yukio Hasegawa, Comparison of force sensors for atomic force microscopy based on quartz tuning forks and length-extensional resonators, *Phys. Rev. B* **84**, 125409 (2011)
- [15] Angelo Peronio and Franz J. Giessibl, Attempts to test an alternative electrodynamic theory of superconductors by low-temperature scanning tunneling and atomic force microscopy, *Phys. Rev. B* **94**, 094503 (2016)
- [16] R. N. Bhargava, de Haas-van Alphen and Galvanomagnetic Effect in Bi and Bi-Pb Alloys, *Phys. Rev.* **156**, 785 (1967).
- [17] Boris J. Albers, Marcus Liebmann, Todd C. Schwendemann, Mehmet Z. Baykara, Markus Heyde, Miquel Salmeron, Eric I. Altman, and Udo D. Schwarz, Combined low-temperature scanning tunneling/atomic force microscope for atomic resolution imaging and site-specific force spectroscopy, *Rev. Sci. Instr.* **79**, 033704 (2008)
- [18] Jens Falter, Marvin Stieffermann, Gernot Langewisch, Philipp Schurig, Hendrik Hölscher, Harald Fuchs, and André Schirmeisen, Calibration of quartz tuning fork spring constants for non-contact atomic force microscopy: direct mechanical measurements and simulations, *Beilstein J. Nanotechnol.* 2014, **5**, 507–516.
- [19] Omur E. Dagdeviren and Udo D. Schwarz, Optimizing qPlus sensor assemblies for simultaneous scanning tunneling and noncontact atomic force microscopy operation based on finite element method analysis, *Beilstein J. Nanotechnol.* 2017, **8**, 657–666.
- [20] Franz J. Giessibl, Noncontact Atomic Force Microscopy, (Springer, 2009, chapter 6)
- [21] Joonho Jang, Investigation of half-quantized fluxoid states in Sr₂RuO₄ mesoscopic superconducting rings, University of Illinois at Urbana-Champaign, 2012
- [22] G. Li, Z. Xiang, F. Yu, T. Asaba, B. Lawson, P. Cai, C. Tinsman, A. Berkley, S. Wolgast, Y. S. Eo, Dae-Jeong Kim, C. Kurdak, J. W. Allen, K. Sun, X. H. Chen, Y. Y. Wang, Z. Fisk, Lu Li, Two-dimensional Fermi surfaces in Kondo insulator SmB₆, *Science* **346**, 1208 (2014)
- [23] E. Morosan, H. W. Zandbergen, Lu Li, Minhyea Lee, J. G. Checkelsky, M. Heinrich, T. Siegrist, N. P. Ong, and R. J. Cava, Sharp switching of the magnetization in Fe_{1/4}TaS₂, *Phys. Rev. B* **75**, 104401 (2007)
- [24] G. Wu, B. L. Kang, Y. L. Li, T. Wu, N. Z. Wang, X. G. Luo, Z. Sun, L. J. Zou, X. H. Chen, Large magnetic anisotropy in Fe_xTaS₂ single crystals, [arXiv:1705.03139](https://arxiv.org/abs/1705.03139)
- [25] J. G. Checkelsky, Minhyea Lee, E. Morosan, R. J. Cava, and N. P. Ong, Anomalous Hall effect and magnetoresistance in the layered ferromagnet Fe_{1/4}TaS₂: The inelastic regime, *Phys. Rev. B* **77**, 014433 (2008)
- [26] Lu Li, Torque Magnetometry in Unconventional Superconductors, Princeton University, 2008
- [27] M. Lee, J. Jahng, K. Kim and W. Jhe, Quantitative atomic force measurement with a quartz tuning fork, *Appl. Phys. Lett.* **91**, 023117 (2007).

- [28] Franz J. Giessibl, Atomic resolution on Si(111)-(7×7) by noncontact atomic force microscopy with a force sensor based on a quartz tuning fork, *Appl. Phys. Lett.* **76**, 1470 (2000)
- [29] D. Shoenberg, *Magnetic oscillations in metals*. (Cambridge University Press, Cambridge, 1984)
- [30] Lu Li, J. G. Checkelsky, Y. S. Hor, C. Uher, A. F. Hebard, R. J. Cava, N. P. Ong, Phase Transitions of Dirac Electrons in Bismuth, *Science* **321**, 547 (2008).
- [31] Yi-han Kao, Cyclotron Resonance Studies of the Fermi Surfaces in Bismuth, *Phys. Rev.* **129**, 1122 (1963)